Thin Solid Films 741 (2022) 139036

Contents lists available at ScienceDirect

Thin Solid Films

journal homepage: www.elsevier.com/locate/tsf

Anti-corrosion behavior of 2-((3-(2-morpholino ethylamino) -N3-((pyridine-2-yl)methyl)propylimino)methyl)pyridine and its reduced form on Carbon Steel in Hydrochloric Acid solution: Experimental and theoretical studies

Majid Rezaeivala [a,*], Saeid Karimi [b], Burak Tuzun [c], Koray Sayin [c]

[a] Department of Chemical Engineering, Hamedan University of Technology, Hamedan, 6516913733, Iran
[b] Department of Metallurgy and Materials Engineering, Hamedan University of Technology, Hamedan, 6516913733, Iran
[c] Sivas Cumhuriyet University, Faculty of Science, Department of Chemistry, 58140 Sivas – TURKEY

ARTICLE INFO

Keywords:
Schiff base
Morpholine
Corrosion behavior
Electrochemical impedance spectroscopy
Acid Inhibition
Modeling studies

ABSTRACT

A comparative investigation of the corrosion inhibition of two ligands, 2-((3-(2-morpholinoethylamino)-N3-((pyridine-2-yl)methyl) propylimino) methyl)pyridine (SB) and N1-(2-morpholinoethyl)-N1,N3-bis(pyridine-2-ylmethyl)propane-1,3-diamine (RSB) for carbon steel in 1.0 M HCl has been carried out. The inhibitor effects on the corrosion behavior of the samples were determined at three different concentrations, 0.1, 1.0 and 2.0 mM. Electrochemical analyses, including corrosion potential and electrochemical impedance spectroscopy (EIS), were utilized to study the corrosion behavior of carbon steel in inhibitor-free and inhibitor-containing electrolytes. The corrosion potential results showed a gradual increment from −450 to −421 mV vs. Ag/AgCl, in the range of 0.2 − 2.0 mM SB concentration. In addition, the corrosion potential of carbon steel in RSB containing solutions is in the range of −439 to −434 mV vs. Ag/AgCl, which results confirm that a higher concentration of SB promotes the inhibition efficiency of samples in 1.0 M HCl solution. The results showed that SB had better inhibition efficiency (around 82.1% at the concentration of 2.0 mM) than RSB. The SB inhibitor exhibited a Langmuir adsorption isotherm, while the adsorption of the RSB did not follow the Langmuir model. EIS studies demonstrated that the addition inhibitors decrease the capacitance of the double layer and increase the resistance of charge transfer. Anticorrosive properties of SB and RSB molecules are examined in detail by using Hartree–Fock (HF) method, Becke, 3-parameter, Lee–Yang–Parr (B3LyP) method, and M062X (highly parameterized, exchange correlation function) methods.

1. Introduction

Carbon steel is widely used in industry due to its ready availability, high strength, and low cost. However, in the presence of acids, carbon steel is highly prone to corrosion [1]. Two main strategies have been considered to prevent corrosion - using a corrosion inhibitor or using alloys that are highly resistant to corrosion [2]. Of these two strategies, using corrosion inhibitors is the better choice due to their availability and greater success in reducing the rate of corrosion of carbon steel in acidic media [1,3-5]. Baddini et al. [6] have evaluated 23 different inhibitors for their anti-corrosion properties on three types of steel, in 15% (w/V) HCl. They found that organic compounds containing oxygen, nitrogen or sulfur atoms were the most efficient corrosion inhibitors [6]. Compounds containing these atoms, particularly those with multiple heteroatoms, can be adsorbed on the surface of the steel replacing adsorbed water molecules and thus reducing corrosive attack in acidic electrolytes [3]. There are many organic compounds that have been discussed and evaluated as inhibitors [7]. Indeed, the choice of the useful inhibitors, and their dosage, for a particular use can be difficult due to the specific nature of the organic inhibitors and the large number of different types of corrosion [3]. To better overcome steel corrosion, there is still a necessity to develop and study substances that can be used as corrosion inhibitors. Schiff bases are versatile compounds which have broad use in pharmaceutical and materials science [5–9]. In coordination chemistry, Schiff bases play an important role as ligands and their complexes have found widespread applications in a number of different

* Corresponding author.
E-mail addresses: mrezaeivala@hut.ac.ir (M. Rezaeivala), s.karimi@hut.ac.ir (S. Karimi).

https://doi.org/10.1016/j.tsf.2021.139036
Received 12 March 2021; Received in revised form 30 November 2021; Accepted 1 December 2021
Available online 5 December 2021

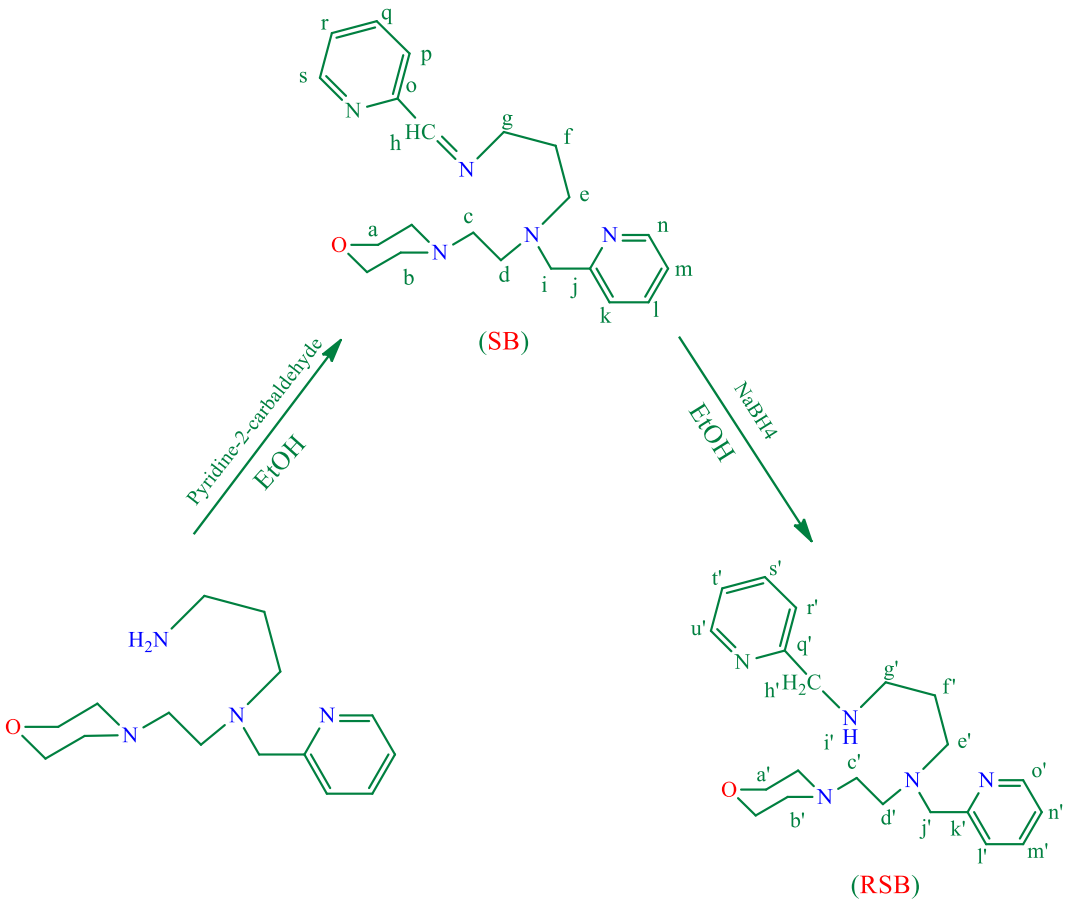

Scheme 1. Synthesis of Schiff base ligand (SB) and related reduced form (RSB).

fields [10–13], such as potent antimicrobial agents [14–17]. In recent years, due to the presence of imine groups in their molecules, Schiff bases have also gained much importance as corrosion inhibitors and potential anti-corrosion agents for many metals because of their excellent inhibition activity, their low cost, ease of synthesis, high synthetic yield and their eco-friendly and less toxic nature [9,18,19]. The objective of the present work is to study the effects of 2-((3-(2-morpholino reduced ethylamino) -N3-((pyridine-2-yl)methyl)propylimino)methyl) pyridine (SB) and its reduced form, N1-(2-morpholinoethyl)-N1,N3-bis (pyridine-2-ylmethyl)propane-1,3-diamine (RSB), as inhibitors on the corrosion of carbon steel in 1.0 M HCl solution by using electrochemical impedance measurements (EIS). In addition to the experimental studies, theoretical studies have been carried out to compare the activities of these molecules as inhibitors [20]. As a result of these theoretical studies, a number of quantum chemical parameters have been obtained, enabling a comparison of the two molecules.

2. Experimental

N1-(2-morpholinoethyl)-N1-((pyridine-2-yl)methyl)propane-1,3-diamine was synthesized according to literature methods [15,16]. Pyridine-2-carbaldehyde and 2-aminoethylmorpholine were purchased from Aldrich Company and used without further purification. The Fourier transform infrared spectroscopy (FT-IR) spectra were recorded on a BIO-RAD FTS-40A spectrophotometer using KBr disks in the region of (4000–400 cm^{-1}). A Bruker 500 spectrometer was employed to determine the ^{1}H and ^{13}CNMR spectra in $CDCl_3$ at room temperature using tetra methyl Silan as internal standard. Mass spectra were measured on Agilent Technology, 5975C VL MSD with triple-Axis detector, Electron Impact (EI) 70 eV. Elemental analysis (C, H, N, S, O) were determined by a Perkin-Elmer model 2400 analyzer.

2.1. Synthesis

2.1.1. Synthesis of SB

N1-(2-morpholinoethyl)-N1-((pyridine-2-yl)methyl)propane-1,3-diamine (0.5 mmol, 0.139 g) in ethanol (20 mL) was added dropwise to stirred solution of pyridine-2-carbaldehyde (0.5 mmol, 0.053 g) in ethanol (50 mL). The mixture was refluxed under stirring for 12 h. A brown oil was obtained that was filtered off, washed with cold ethanol and dried in vacuo.Yield: (80%). Anal. Calc. for $C_{21}H_{29}N_5O$: C, 68.63; H, 7.95; N, 19.06. Found: C, 69.01; H, 7.83; N, 19.32%. IR (KBr, cm^{-1}): 3423, 1649 υ(C = N), 1588, 1469 υ(C = C). (Electron-Impact Mass Spectroscopy)EI-MS (*m/z*): Calc: 367.4879, Found:368.00 $[L]^{+}$. ^{1}H NMR ($CDCl_3$, ppm) δ=1.80 (p, 2H, H-f); 2.26 (t, 4H, H-b); 2.35 (t, 2H, H-e); 2.52 (t, 2H, H-c); 2.57 (t, 2H, H-d); 3.52 (t, 2H, H-g); 3.55 (t, 4H, H-a); 3.66 (s, 2H, H-i); 6.96 (t, 1H, H-m); 7.17 (t, 1H, H-k); 7.38 (d, 1H, H-r); 7.48 (t, 1H, H-l); 7.59 (t, 1H, H-q); 7.80 (d, 1H, H-p); 8.23(s, 1H, H-h); 8.35 (d, 1H, H-n); 8.50 (d, 1H, H-s). ^{13}C NMR ($CDCl_3$, ppm) δ=28.08 (c-f); 51.25 (c-e); 52.27 (c-c); 53.94 (c-d); 56.86 (c-b); 59.06 (c-g); 60.76 (c-i); 66.77 (c-a); 121.06 (c-p); 121.71 (c-m); 122.76 (c-k); 124.55 (c-r); 136.22 (c-q); 148.71 (c-n); 149.24 (c-s); 154.37 (c-h); 160.12 (c-j); 161.87(c-o) (Scheme 1).

2.1.2. Synthesis of RSB

To an ethanlic solution (50 mL) of 2-((3-(2-morpholinoethylamino)-N3-((pyridine-2-yl)methyl) propylimino) methyl)pyridine (0.5 mmol, 0.183 g) was added slowly sodium borhydride (0.25 mmol, 0.009 g). The mixture was refluxed under stirring for 12 h. A brown oil was obtained that was filtered off, washed with ethanol and dried in vacuo. Yield: (87%). Anal. Calc. for $C_{21}H_{31}N_5O$: C, 68.26; H, 8.46; N, 18.95. Found: C, 68.46; H, 8.31; N, 19.02%. IR (KBr, cm^{-1}): 3386 $υ(N—H)_{str}$, 1671 $υ(N—H)_b$, 1596, 1433 υ(C = C). EI-MS (*m/z*): Calc: 369.5037,

Table 1
Chemical composition (in wt.%) of the base metal.

Elements	C	Si	Ni	Mn	P	Cr
wt.%	0.049	0.010	0.003	0.221	0.013	0.001

Found: 369.00 $[L]^+$. ^{1}H NMR ($CDCl_3$, ppm) δ=1.69 (p, 2H, H-f'); 2.33 (t, 4H, H-b'); 2.42 (t, 2H, H-e'); 2.54 (t, 2H, H-c'); 2.59 (t, 2H, H-d'); 3.59 (t, 2H, H-g'); 3.62 (t, 4H, H-a'); 3.69 (s, 2H, H-I'); 3.83 (s, 2H, H-h'); 7.06 (t, 1H, H-m'); 7.08 (t, 1H, H-k'); 7.25 (d, 1H, H-r'); 7.39 (t, 1H, H-l'); 7.54 (t, 1H, H-q'); 7.56 (d, 1H, H-p'); 8.41 (d, 1H, H-n'); 8.46 (d, 1H, H-s'). ^{13}C NMR ($CDCl_3$, ppm) δ=27.29 (c-f'); 47.93 (c-g'); 51.14 (c-h'); 52.90 (c-d'); 53.99 (c-c'); 55.18 (c-b'); 56.84 (c-j'); 60.80 (c-e'); 66.80 (c-a'); 121.80 (c-n'); 121.88 (c-s'); 122.26 (c-l'); 122.86 (c-q'); 136.29 (c-m'); 136.36 (c-r'); 148.80 (c-o'); 149.14 (c-t'); 159.55 (c-k'); 160.07(c-p') (Scheme 1).

2.2. Theoretical studies

Gaussian software program was used for the theoretical calculations [21]. Quantum chemical calculations of studied compounds were done by aid of the Hartree–Fock (HF) method, Becke, 3-parameter, Lee–Yang–Parr (B3LyP) method, and M062X (highly parameterized, exchange correlation function) methods with 6–31 g basis set. Some quantum chemical parameters which are E_{HOMO} (Highest Occupied Molecular Orbital), E_{LUMO} (Lowest Unoccupied Molecular Orbital), ΔE (energy gap between HOMO and LUMO), electronegativity (χ), chemical potential (μ), chemical hardness (η), electrophilicity (ω), nucleophilicity (ε), global softness (σ) and proton affinity [22–24], are calculated to determine the anticorrosive properties of studied compounds.

2.3. Solutions, electrodes and electrochemical experiments

Electrochemical measurements were carried out using a conventional three-electrode-electrochemical cell using a Iviumstat compact 20,250 H Potentiostat controlled by Ivium soft electrochemistry software and, a GSTAT101N Potentiostat (Metrohm Autolab) controlled by Nova software (Version 2.1.4). Carbon steel having the chemical composition as shown in Table 1 was used as the working electrode. An Ag/AgCl electrode (Metrohm Ag) filled with saturated KCl (217 mV vs. SHE at 22 °C) and a platinum electrode was used as reference and counter electrodes, respectively. Before electrochemical testing, the working electrode was cold-mounted in an epoxy resin after being connected to a copper wire. The steel electrodes were ground wet with 1500 grit SiC to give a smooth surface, and this was followed by rinsing with acetone and ethanol and finally dried in hot air. The testing solution used for all the experiments was 1.0 M hydrochloric acid, prepared by dilution of analytical grade 37% hydrochloric acid with distilled water. The electrochemical experiments were carried out at atmospheric pressure and with the temperature maintained at 22 °C; the solutions were not stirred. The concentration of SB and RSB varied within the range of 0.2 − 2.0 mM.

To ensure reproducibility, measurements began only after the corrosion potential was reached, to within ±5 mV. Electrochemical impedance spectroscopy measurements were conducted at corrosion potential, in the range of 10^{-1}–10^5 Hz with peak–to–peak amplitude of 10 mV. Each electrochemical experiment was repeated at least twice to ensure the reproducibility of results.

3. Results and discussions

3.1. Characterization of SB and RSB

3.1.1. FT-IR and mass spectra

A Schiff base ligand, (SB) has been prepared through the condensation reaction of N1-(2-morpholinoethyl)-N1-((pyridine-2-yl)methyl) propane-1,3-diamine and pyridine-2-carbaldehyde, with a molar ratio of 1:1, for 6 h in ethanol. The prepared Schiff base was characterized by CHN elemental analysis and by spectroscopic techniques. The FT-IR spectrum of the Schiff base ligand (SB), showed a sharp band at 1649 cm^{-1} related to the stretching vibration frequency of the imine group, indicating the condensation of the precursors to produce the Schiff base ligand. The mass spectrum of the SB showed the molecular ion peak at $m/z = 368$ which is consistent with the proposed molecular formula. The RSB was prepared by an in-situ reduction of the Schiff-base ligand, and characterized by microanalysis, IR, EI-MS and ^{1}H and ^{13}C NMR spectroscopy. The IR spectrum shows bands at 1596, 1569 and 1433 cm^{-1}, associated with the υ(C = N) and υ(C = C) vibrations from the pyridine ring. The υ(N–H) band appears at 3386 cm^{-1}. The mass spectrum of RSB showed the molecular ion peak at $m/z = 369$ which is consistent with the proposed molecular formula.

3.1.2. NMR spectral studies

The ^{1}H and ^{13}C NMR spectra of the compounds were recorded in $CDCl_3$. The peaks obtained were consistent with the structures of the synthesized Schiff base compound and its reduced compound. For both compounds the aromatic protons appeared as multiples between 6.98–8.50 ppm. The imino proton, for SB, was observed at 8.23 ppm, while in the reduced form, the singlet at δ 3.83, due to $–CH_2$- group, confirms the formation of the reduced Schiff base. The ^{13}C NMR spectrum showed the signals due the methyl carbon at 51.14 ppm, and the peaks which appeared in the range 114.17–159.24 ppm reflect the aromatic carbons. The signal due to the imino carbon, in SB, appeared at 154.37 ppm.

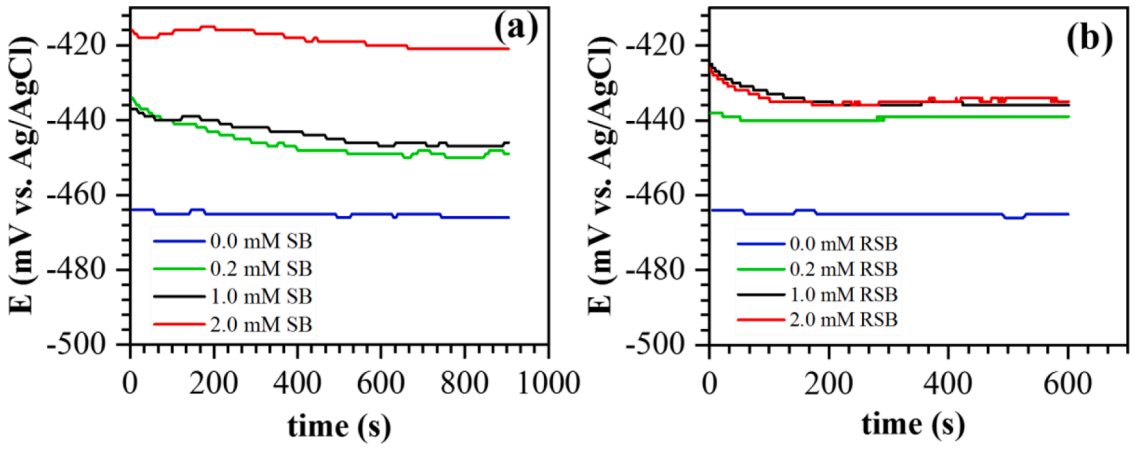

Fig. 1. The corrosion potential value of carbon steel in 1.0 M HCl at different concentration of (a) SB and (b) RSB.

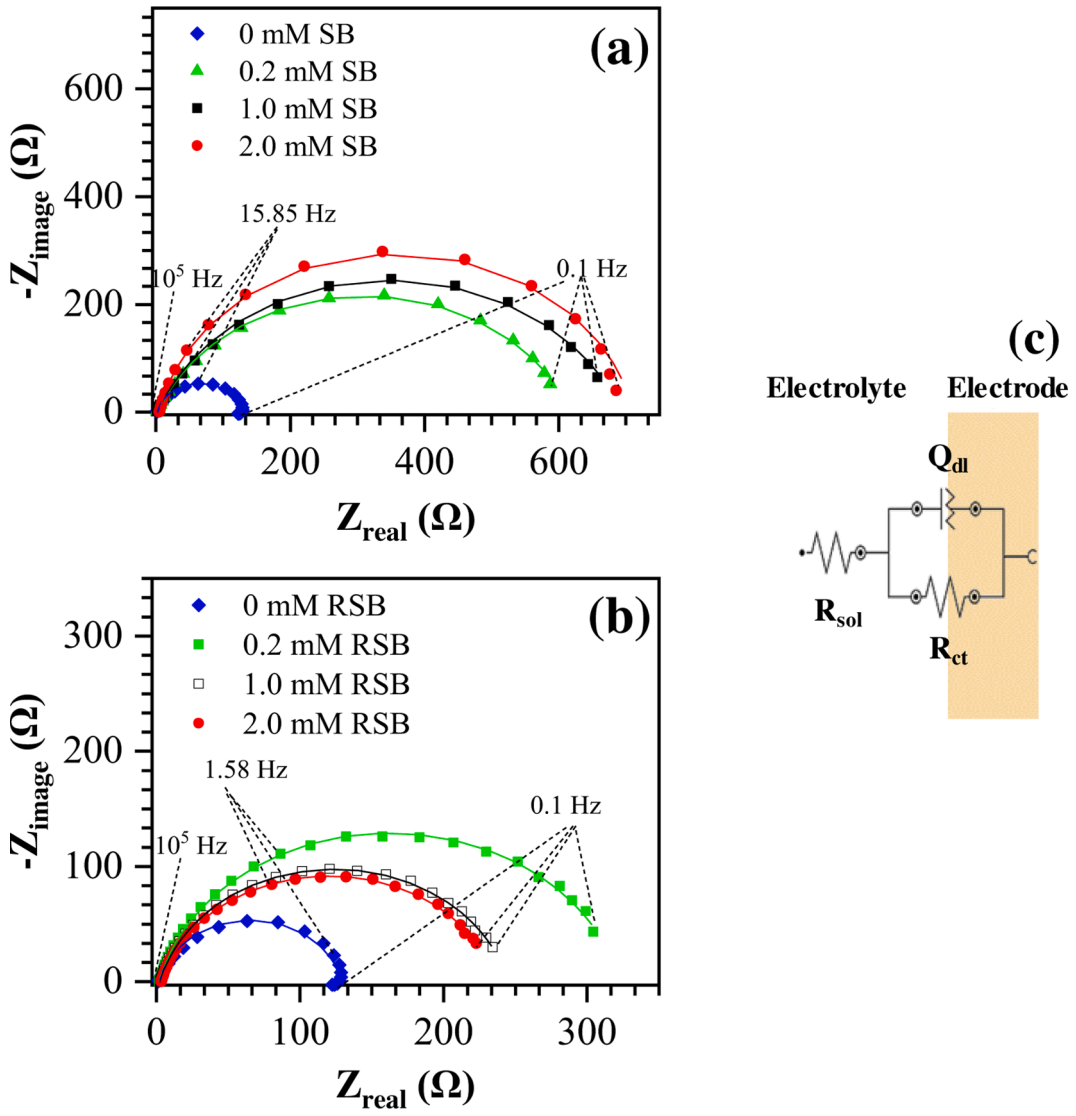

Fig. 2. Measured and simulated Nyquist impedance spectra of carbon steel at corrosion potential 1.0 M HCl at different concentrations of (a) SB and (b) RSB, and (c) schematic of an equivalent circuit on the electrode surface.

3.2. Corrosion behavior

3.2.1. Corrosion potential measurements

To ensure the reproducibility of all the electrochemical tests, the working electrode was allowed to reach the corrosion potential. The corrosion potential magnitude of the samples is thermodynamic parameters which is a precise indication of their tendency of those materials to participate in the corrosion reactions with the surrounding media. It has been found that a carbon steel electrode with a higher noble corrosion potential will be more thermodynamically stable than that electrode has a less noble corrosion potential in a solution [8]. The corrosion potential evolution of the carbon steel electrode in 1.0 M HCl solution, in the absence and presence of different concentrations of SB and RSB, is shown in Fig 1. The corrosion potential of carbon steel generally reached a steady-state condition in a few seconds after being immersed in the solutions. As depicted in Fig. 1a, the corrosion potential of carbon steel in solutions containing SB shows a higher value in than is found in a SB free solution, indicating higher inhibition activity in the solutions containing SB. The corrosion potential value gradually increases from −450 to −421 mV vs. Ag/AgCl with increasing SB concentration, in the range of 0.2 − 2.0 mM. These results confirm that a higher concentration of SB promotes thermodynamic stability of samples in 1.0 M HCl solution. It is evident that the corrosion potential of carbon steel in RSB containing solutions is in the range of −439 to −434 mV vs. Ag/AgCl, a somewhat narrower potential range than the SB containing solutions. It can be seen that increasing the concentration of RSB from 1.0 to 2.0 mM, in 1.0 M HCl solution, does not make much difference in the resulting corrosion potential values and thus it can be concluded that concentrations of RSB greater than 1.0 mM no longer affects the electrochemical activity and surface characteristics of the carbon steel electrodes. Additionally, the corrosion potential value for 0.2 and 1.0 mM SB containing solutions are very close to the corresponding RSB containing solutions. The carbon steel electrode in the 2 mM SB-containing solution showed the highest corrosion potential value giving rise to the highest thermodynamic stability compared to the other samples with varying SB and RSB concentrations.

3.2.2. Electrochemical impedance spectroscopy study

Fig. 2a and 2b show the measured and simulated Nyquist impedance spectra of carbon steel at the corrosion potential, in both absence and presence of the inhibitors SB and RSB. Only one time constant can be seen in the testing frequency range for the samples in 1.0 M HCl, with and without inhibitors, which is generally attributed to a process mainly controlled by charge transfer. The Nyquist diagram obtained in the

Table 2
Model parameters for an equivalent circuit of Fig. 2c.

Inhibitor type	Concentration (mM)	$R_{sol.}$ (Ω cm^2)	R_{ct} (Ω cm^2)	Q_{dl} Y_0 (Ω s^{-n})	n	χ^2
Inhibitor-free	0.0	2.41	126.06	1.31×10^{-4}	0.89	0.013
SB	0.2	2.68	615.90	2.37×10^{-4}	0.78	0.010
	1.0	2.68	690.40	2.33×10^{-4}	0.79	0.011
	2.0	5.27	705.55	2.00×10^{-4}	0.81	0.012
RSB	0.2	2.07	321.00	8.11×10^{-4}	0.86	0.005
	1.0	2.79	241.70	8.67×10^{-4}	0.86	0.003
	2.0	3.34	233.60	9.50×10^{-4}	0.85	0.002

absence and presence of different concentrations of SB and its reduced form corresponded to the double-layer capacitive impedance with a charge transfer resistance in the interface of the carbon steel electrode/electrolyte. It is worth mentioning that the shape of Nyquist diagrams is a depressed semi-circle and has the deviation from an ideal behavior of a capacitance. This phenomenon illustrates use of the constant phase element (CPE), which includes two electrochemical parameters: Y_0 (the admittance of CPE) and n (empirical constant). The value smaller than 1.0 arises from the roughness of the carbon steel surface and inhomogeneity owing to the adsorption of inhibitors together with the product of the corrosion process [9].

The equivalent electrical circuit is depicted in Fig. 2c, and its electrical parameters are shown in Table 2. An equivalent electrical circuit designed to fit the EIS diagrams contains a solution resistance ($R_{sol.}$) in series with Q_{dl}/R_{ct}.

As already known, charge transfer resistance is a characteristic quantity for corrosion resistance, as the higher the charge transfer resistance, the higher the corrosion resistance. From the charge transfer resistance values given in Table 2, the resistance obtained in the presence of SB was quite higher than that in the absence of SB (126.06 Ω cm^2). Also, the trend for efficiency of inhibition for SB inhibitor follows the order of 2.0 mM > 1.0 mM > 0.2 mM. The charge transfer resistance for carbon steel in SB-containing solution increases significantly from 615.90 to 705.55 Ω cm^2 by promoting a concentration of from 0.2 to 2.0 mM of the SB. It is apparent from the data in Table 2 that on increasing the RSB concentration, a decrement in the value of R_{ct} is observed (321 to 233 Ω cm^2). Also, the EIS data for inhibitors confirms that SB-containing solutions have much better corrosion resistance for carbon steel than that for RSB compound.

Generally, an increase in inhibitor concentration leads to an increment of the thickness and surface coverage of the adsorbed material in the inhibitor layer, which is effectively adsorbed on the electrode surface; the inhibitor replaces water molecules adsorbed on the carbon steel surface [25,26].

$$Org_{(sol)} + aH_2O_{(ads)} \leftrightarrow Org_{(ads)} + aH_2O_{(sol)} \quad (1)$$

The inhibitory efficiency of Schiff bases is related to the structural nature of the Schiff bases with Nitrogen, Sulfur, Oxygen and Phosphorous heteroatoms in the molecules, which serve as reaction cores for physical adsorption on the substrate surface. The transfer of electrons from these compounds to the substrate surface is facilitated by the availability of lone pairs and p-electrons in the organic molecules, leading to the formation of coordinate covalent or non-covalent bonds with the metals. Previous research indicates in some cases, the imine group is not stable, particularly in acid medium, where it undergoes hydrolysis, regenerating an amine and an aldehyde [27]. In this work the experimental results indicate that the Schiff base compound, with two pyridine groups, is stable in acidic solution.

Table 3
The capacitance of double layer and inhibition efficiency values of carbon steel in 1.0 M HCl solution containing different concentrations of inhibitors.

Inhibitor type	No Inhibitor	SB			RSB		
	1.0 M HCl	0.2 mM	1.0 mM	2.0 mM	0.2 mM	1.0 mM	2.0 mM
C_{dl} (μF cm^{-2})	789.9	216.3	143.4	126.3	651.4	672.2	728.4
IE (%)	–	79.5	81.7	82.1	60.7	47.8	46.0

The lower capacitance of double layer can be evidence of the higher efficiency of the inhibitor. The value of the double layer capacitance is calculated by the following equation [28]:

$$C_{dl} = \left(\frac{Y_0}{R_{ct}^{n-1}}\right)^{\frac{1}{n}} \quad (2)$$

where C_{dl} is capacitive of double layer, Y_0 represents the value of CPE, R_{ct} is the charge transfer resistance and, n is the phase exponent, which is always in the range of 0 to 1. As the following equation, C_{dl} is inversely proportional to the thickness of the double-layer, which serves as a barrier layer for protection from corrosion.

$$C_{dl} = \frac{\varepsilon\varepsilon_0 A}{d} \quad (3)$$

where ε is dielectric constant, ε_0 is vacuum permittivity, d is the thickness of the electrical double layer and, A is electrode area in the electrolyte. It is clear from the data in Table 3, an increase in SB concentration leads to a gradual decrease in the value of double layer capacitance (216.3 to 126.3 μF cm^{-2}), which implies a reduction in dielectric constant and/or an increase in the double-layer thickness [9]. These results indicate that the presence of SB leads to the decrease in capacitance of the double-layer due to the replacement of H_2O molecules by inhibitor ions at the surface of the carbon steel electrode. As a result of the adsorption of inhibitors on the electrode surface, the effective value of area (A), which can intensify corrosion rate, decreases, and the efficiency of surface protection is increased. The adsorption of SB molecules on the electrode surface acts as a barrier for ions and charge transfers between metal and electrolyte; thus, enhancing the protecting surface from corrosion. These findings confirm the data obtained in EIS analysis, in which higher charge transfer resistance led to higher protection efficiency while the C_{dl} for carbon steel in RSB containing solutions increases from 651.4 to 728.4 μF cm^{-2} by increasing the inhibitor concentration. Despite relatively adequate corrosion protection of carbon steel in a solution containing RSB, compared to an inhibitor-free solution, RSB shows a less perfect protective layer on the carbon steel compared to SB.

Table 3 also shows the inhibition efficiency (IE) calculated from charge transfer resistance values obtained in EIS diagrams shown in Fig. 2 as follows:

$$IE(\%) = \frac{R_{ct} - R_{ct}^0}{R_{ct}} \times 100 \quad (4)$$

where R_{ct} and R_{ct}^0present the charge transfer resistance of carbon steel with and without inhibitors, respectively. The IE increases by adding more SB-inhibitor with a maximum IE of 82.1% at 2.0 mM concentration. As can be seen in Table 3, there is a gradual increment in the efficiency of inhibition of SB containing solution from 79.5% to 82.1%, which represents only a 2.6% improvement in corrosion protection by increasing inhibitor concentration from 0.2 mM to 2 mM (tenfold increase in inhibitor concentration).

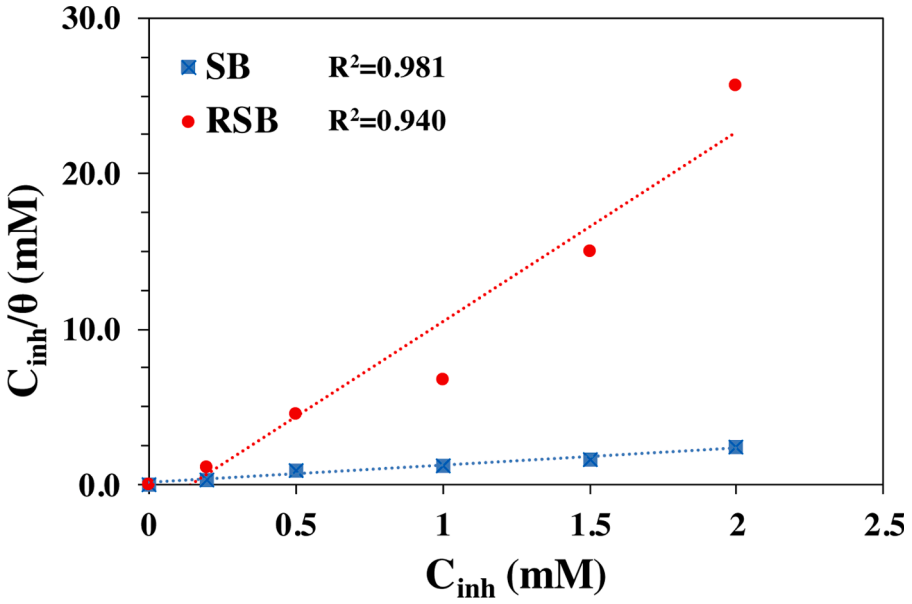

Fig. 3. Langmuir adsorption isotherms involving SB and its reduced form (RSB).

3.3. Adsorption mechanism

The adsorption of inhibitor on the surface of the carbon steel electrode is the vital step in an inhibition mechanism [5]. The main reason for higher corrosion protection in the presence of inhibitors is the adsorption of this material on the carbon steel surface. Based on the previous studies [3,22], the Langmuir adsorption model is the best model to explain the adsorption process of the SB and RSB inhibitors on the surface of carbon steel in 1.0 M HCl. The Langmuir adsorption isotherm, which is based on a simple kinetics model for monolayer adsorption on localized adsorption sites, is presented as follows:

$$\frac{C_{inh}}{\theta} = \frac{1}{K_{ads}} + C_{inh} \tag{5}$$

where C_{inh} is the concentration of inhibitor, K_{ads} the adsorption equilibrium constant and θ the fraction of surface coverage by the inhibitor molecule, which is calculated by the following equation [29]:

$$\theta = 1 - \frac{C_{dl}^{i}}{C_{dl}^{b}} \tag{6}$$

where C_{dl}^{i} is the capacitive response of the carbon steel electrode resulted in the containing inhibitor and C_{dl}^{b} is the capacitive of double layer in free-inhibitor solution. Langmuir relationship, a plot of C_{inh}/θ against C_{inh} should yield a straight line via the regression coefficient, R^2 (shown in Fig. 3). The R^2 values give a good agreement between the EIS and Langmuir data for SB (R^2 =0.981) and RSB (R^2 =0.940) inhibitors. The near unity slope for SB containing solution (i.e., slope=1.11) supports the suitability of the Langmuir model for obtained results in the present study. However, the slope for RSB containing solution was 12.23 which showed a deviation from 1.0, suggesting a more complex adsorption phenomenon than just a simple monolayer formation.

The value of K_{ads} can be calculated by considering the width of the original value of the C_{inh}/θ against C_{inh} diagrams. The K_{ads} obtained for SB and RSB inhibitors are 105.7 and 5.65 $(mM)^{-1}$, respectively. The Langmuir K_{ads} value can be interpreted as the adsorption/desorption equilibrium for each inhibitor on the surface of carbon steel. In other words, it describes the fraction of the electrode surface, which is covered by inhibitor molecules. The higher the adsorption equilibrium constant, the more corrosion protection there appears to be.

Furthermore, it is noting that valuable information about the mechanism of corrosion inhibition of carbon steel can be obtained by calculating the standard Gibbs free energy (ΔG_{ads}^{0}) in adsorption isotherm phenomena. The type of interaction between electrode surface and inhibitor molecules can be characterized by usingΔG_{ads}^{0}. The free Gibbs energy was measured by the following equation [30]:

$$\Delta G_{ads}^{0} = -RT\ln(55.5K_{ads}) \tag{7}$$

where 55.5 demonstrates the concentration of water in the solution in M, T is the temperature in K, R the universal gas constant 8.314 $J.mol^{-1}.K^{-1}$. The values of Gibbs energy for the adsorption of inhibitor on the metals surface were found to be −21.5 kJ/mol and −14.2 kJ/mol, representing that the inhibitor molecules are electrostatically adsorbed on electrode surface. In general, values of the Gibbs energy less than −40 kJ/mol are related to the inhibiting processes that take place by physical adsorption on the electrode surface.

3.4. Computational chemistry

As a result of theoretical calculations, many quantum chemical parameters have been calculated. Each calculated quantum chemical parameter allows us to comment on the different chemical properties of molecules. Among these calculated parameters, the most important parameters are E_{HOMO} and E_{LUMO}, which are used to explain the electron transfer between the inhibitor molecules and the metal surface. The molecule with the highest E_{HOMO} energy value of the inhibitor molecules has the highest inhibitory activity. Because of the E_{HOMO} energy value shows the ability of molecules to donate electrons. The molecule with the highest energy of the E_{HOMO} (Highest Occupied Molecular Orbital) of the molecules donates electrons more easily than other molecules. On the other hand, the inhibitory activity of the molecule with the lowest E_{LUMO} energy value is higher than the other molecules. Because of the E_{LUMO} energy value indicates the electron accepting ability of molecules. The molecule with the lowest energy of the E_{LUMO} (Lowest Unoccupied Molecular Orbital) of the molecules accepts electrons more easily than other molecules. Many other parameters calculated have a similar order since they are calculated from the HOMO and LUMO parameter of the molecules.

When the HOMO values obtained in the calculations are examined, it is seen that the molecule SB is −9.1374 at the HF/6–31 g level, −6.0916 at the B3LYP/6–31 g level and −7.7915 at the M062X/6–31 g level. On the other hand, the molecule RSB was found to be −9.0990 at HF/6–31 g

Table 4
The calculated quantum chemical parameters of molecules.

	E_{HOMO}	E_{LUMO}	I	A	ΔE	η	σ	χ	Pİ	ω	ε	dipole	Energy
HF/6–31 g LEVEL													
SB	−9.1374	1.0033	9.1374	−1.0033	10.1407	5.0703	0.1972	4.0670	−4.0670	1.6311	0.6131	2.8890	−31,532.5902
RSB	−9.0990	0.9023	9.0990	−0.9023	10.0014	5.0007	0.2000	4.0983	−4.0983	1.6794	0.5954	3.7871	−31,563.7367
B3LYP/6–31 g LEVEL													
SB	−6.0916	−1.8028	6.0916	1.8028	4.2888	2.1444	0.4663	3.9472	−3.9472	3.6328	0.2753	3.0619	−31,736.5589
RSB	−6.0881	−1.0694	6.0881	1.0694	5.0186	2.5093	0.3985	3.5787	−3.5787	2.5520	0.3919	3.5393	−31,768.9028
M062X/6–31 g LEVEL													
SB	−7.7915	−0.7489	7.7915	0.7489	7.0426	3.5213	0.2840	4.2702	−4.2702	2.5892	0.3862	2.7510	−31,722.1921
RSB	−7.7896	−0.3761	7.7896	0.3761	7.4135	3.7068	0.2698	4.0828	−4.0828	2.2485	0.4447	3.6208	−31,754.4202

Table 5
The calculated quantum chemical parameters of protonated form of molecules.

	E_{HOMO}	E_{LUMO}	I	A	ΔE	η	σ	χ	Pİ	ω	ε	dipole	Energy
HF/6–31 g LEVEL													
SB	−8.2666	−5.0807	8.2666	5.0807	3.1859	1.5930	0.6278	6.6736	−6.6736	13.9794	0.0715	19.3322	−31,745.2556
RSB	−7.9159	−4.8537	7.9159	4.8537	3.0621	1.5311	0.6531	6.3848	−6.3848	13.3129	0.0751	15.2550	−31,777.6143
B3LYP/6–31 g LEVEL													
SB	−10.6629	−2.4322	10.6629	2.4322	8.2307	4.1153	0.2430	6.5475	−6.5475	5.2086	0.1920	21.3007	−31,541.3660
RSB	−11.5100	−2.1402	11.5100	2.1402	9.3698	4.6849	0.2135	6.8251	−6.8251	4.9715	0.2011	9.8913	−31,572.5898
M062X/6–31 g LEVEL													
SB	−9.3352	−4.0537	9.3352	4.0537	5.2815	2.6407	0.3787	6.6945	−6.6945	8.4854	0.1178	11.5782	−31,730.8317
RSB	−9.9276	−3.8107	9.9276	3.8107	6.1169	3.0584	0.3270	6.8692	−6.8692	7.7139	0.1296	10.2417	−31,763.4768

level, −6.0881 at B3LYP/6–31 g level and −7.7896 at M062X/6–31 g level. Considering the HOMO values of the molecules, it was observed that the HOMO energy value of the RSB molecule was higher than that of the SB molecule. Therefore, the inhibitory activity of RSB is higher. However, the RSB LUMO energy values are lower than those of the SB. The activity of RSB is higher at the HF/6–31 g level.

All parameters found as a result of calculations are given in Table 4. Other parameters given in this table are calculated from the HOMO and LUMO energy values of the inhibitor molecules. The HOMO parameter of inhibitor molecules indicates the electron donating ability of the molecules. Molecular being a better inhibitor depends on their ability to donate electrons more easily. In order for the molecules to donate electrons more easily, they must have a higher HOMO energy value. As can be seen from Table 4, the values for E_{HOMO} for the HF, B3LYP and

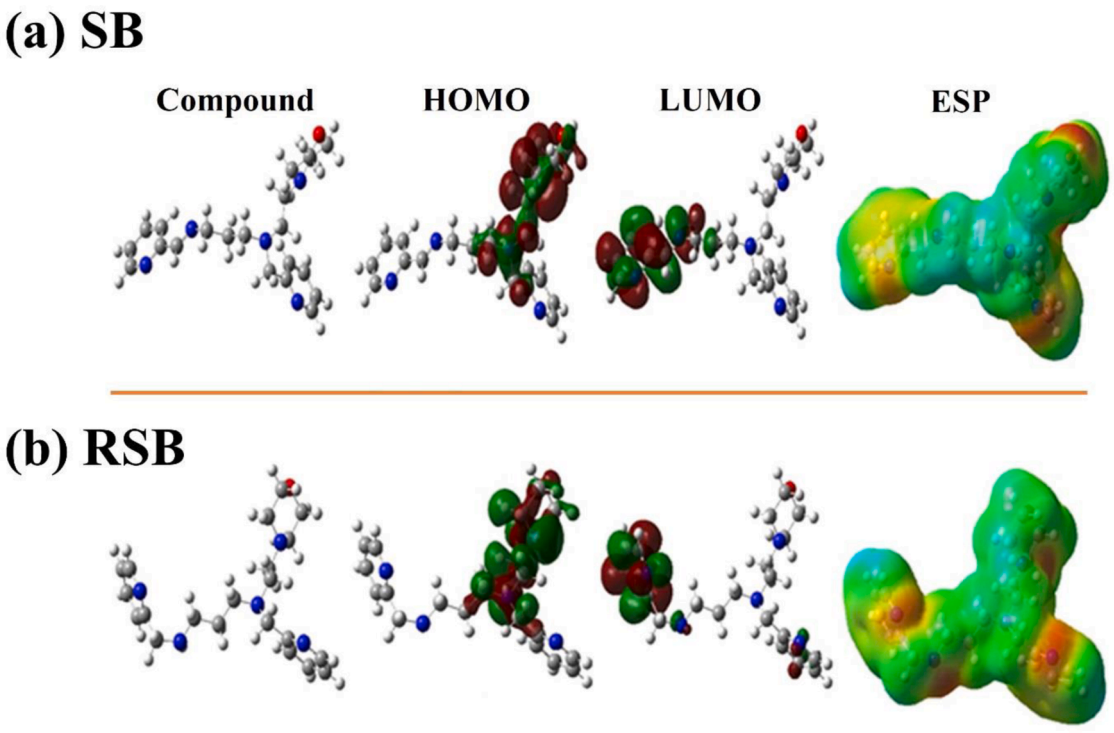

Fig. 4. A representation of optimized structures, HOMO, LUMO, and ESP shapes of inhibitor molecules (a) SB and (b) RSB.

M062X are different, but are consistent with the values for RSB being higher than for SB; this suggests that RSB should have a higher inhibition activity. In contrast, the E_{LUMO} values for RSB are lower than SB only at the HF level; at the B3LYP and M062 level the values for SB are lower than RSB, suggesting that, on average, SB should have a higher inhibition activity. The LUMO parameter of inhibitor molecules indicates the electron accepting ability of the molecules. The molecular ability to be a better inhibitor depends on their easier electron acceptability. For molecules to accept electrons more easily, they must have a lower LUMO energy value. As a result of the calculations, the numerical value of the HOMO energy of the RSB molecule was higher in the B3LYP and HF basis sets. As can be seen from the explanations above, the higher the HOMO energy value, the higher the inhibitory activity of the molecule. On the other hand, when the LUMO energy values are examined, the LUMO energy value of the RSB molecule in the HF basis set is lower than the other molecule. Compared to the LUMO energy value of the RSB molecule, its inhibitory activity is higher. Most of the theoretical calculations made are in agreement with the experimental results. But the most important reason why there are some minor differences is that the theoretical calculations are made in a pure and isolated environment. On the other hand, there are some differences between experimental and theoretical calculations because there are many experimental inputs in experimental processes. Table 5

The compound, HOMO, LUMO and ESP (Molecular electrostatic potential) of inhibitor molecules are given in Fig. 4a (SB) and b (RSB) (in order from left to right). In Fig. 4, the optimized structures (compound) of both inhibitor molecules are given. The second and third pictures show the atoms on which the HOMO and LUMO orbitals of the inhibitor molecules are located on. In the last picture, ESP diagrams of the inhibitor molecules are given. In this picture, the red-colored regions have a high electron density while the blue-colored regions have low electron density.

4. Conclusion

The corrosion behavior of carbon steel in 1.0 M HCl in the presence and absence of inhibitors was investigated by using electrochemical techniques. The addition of SB and RSB inhibitors to the 1.0 M HCl electrolyte decrease corrosion of steel. The compound SB was found to show a better inhibitor characteristic than RSB. The inhibition efficiency of SB increases with increasing concentration and gives the highest value at a concentration of 2.0 mM (e.g., 82.1%), whereas the rate corrosion of carbon steel tends to increase by an increment of RSB and presented a minimum rate at 0.1 mM in the range of 0.1–2.0 mM. EIS measurements indicated that with increasing concentration of SB, the charge transfer resistance (R_{ct}) increased while the capacitance of the double layer (C_{dl}) decreased. The adsorption of SB molecules on the surface of carbon steel follows a Langmuir adsorption isotherm, while the adsorption of RSB shows a significant deviation from a Langmuir isotherm. The theoretical calculations of the inhibitor molecules suggest that the activity of the RSB inhibitor molecule should higher than for SB. These differences are due to the theoretical calculations being carried on isolated molecules in the gas phase, rather than the molecules being adsorbed on the surface of the carbon steel. With these theoretical comparisons, more effective and more active inhibitors are used to synthesize.

CRediT authorship contribution statement

Majid Rezaeivala: Conceptualization, Writing – review & editing. **Saeid Karimi:** Data curation, Methodology, Writing – review & editing. **Burak Tuzun:** Software. **Koray Sayin:** Software, Investigation, Validation.

Declaration of Competing Interest

The authors declare that they have no known competing financial interests or personal relationships that could have appeared to influence the work reported in this paper.

Acknowledgement

We thank Hamedan University of Technology. Also, this work was supported by Research Fund of TÜBİTAK ULAKBİM High Performance and Grid Computing Center (TR-Grid e-Infrastructure). The authors would like to thank Dr. Robert W. Gable, University of Melbourne, for constructive criticism of the manuscript.

References

[1] H. Jafari, K. Sayin, Sulfur Containing Compounds as Corrosion Inhibitors for Mild Steel in Hydrochloric Acid Solution, Trans. Indian Inst. Met. 69 (2016) 805–815, https://doi.org/10.1007/s12666-015-0556-2.
[2] E. Hart, Corrosion inhibitors: principles, mechanisms and applications, 2016. https://doi.org/10.5772/57255.
[3] A.B. da Silva, E. D'Elia, J.A. da Cunha Ponciano Gomes, Carbon steel corrosion inhibition in hydrochloric acid solution using a reduced Schiff base of ethylenediamine, Corros. Sci. 52 (2010) 788–793, https://doi.org/10.1016/j.corsci.2009.10.038.
[4] R. Rihan, R. Shawabkeh, N. Al-Bakr, The effect of two amine-based corrosion inhibitors in improving the corrosion resistance of carbon steel in sea water, J. Mater. Eng. Perform. 23 (2014) 693–699, https://doi.org/10.1007/s11665-013-0790-x.
[5] H. Jafari, F. mohsenifar, K. Sayin, Corrosion inhibition studies of N,N'-bis(4-formylphenol)-1,2-Diaminocyclohexane on steel in 1 HCl solution acid, J. Taiwan Inst. Chem. Eng. 64 (2016) 314–324, https://doi.org/10.1016/j.jtice.2016.04.021.
[6] A.L. de Q. Baddini, S.P. Cardoso, E. Hollauer, J.A. da C.P. Gomes, Statistical analysis of a corrosion inhibitor family on three steel surfaces (duplex, super-13 and carbon) in hydrochloric acid solutions, Electrochim. Acta. 53 (2007) 434–446, https://doi.org/10.1016/j.electacta.2007.06.050.
[7] Z. Tang, A review of corrosion inhibitors for rust preventative fluids, Curr. Opin. Solid State Mater. Sci. 23 (2019), 100759, https://doi.org/10.1016/j.cossms.2019.06.003.
[8] S. Karimi, A. Ghahreman, F. Rashchi, Kinetics of Fe(III)-Fe(II) redox half-reactions on sphalerite surface, Electrochim. Acta. 281 (2018) 624–637, https://doi.org/10.1016/j.electacta.2018.05.132.
[9] B. Chugh, A.K. Singh, S. Thakur, B. Pani, H. Lgaz, I.M. Chung, R. Jha, E.E. Ebenso, Comparative Investigation of Corrosion-Mitigating Behavior of Thiadiazole-Derived Bis-Schiff Bases for Mild Steel in Acid Medium: experimental, Theoretical, and Surface Study, ACS Omega 5 (2020) 13503–13520, https://doi.org/10.1021/acsomega.9b04274.
[10] S. Vikneshvaran, S. Velmathi, Impact of Halide-Substituted Chiral Schiff Bases on Corrosion Behaviour of Carbon Steel in Acidic Environment, J. Nanosci. Nanotechnol. 19 (2019) 4458–4464, https://doi.org/10.1166/jnn.2019.16367.
[11] K. Nejati, Z. Rezvani, B. Massoumi, Syntheses and investigation of thermal properties of copper complexes with azo-containing Schiff-base dyes, Dye. Pigment. (2007), https://doi.org/10.1016/j.dyepig.2006.07.019.
[12] M. Rezaeivala, H. Keypour, Schiff base and non-Schiff base macrocyclic ligands and complexes incorporating the pyridine moiety - The first 50 years, Coord. Chem. Rev. 280 (2014) 203–253, https://doi.org/10.1016/j.ccr.2014.06.007.
[13] M. Shariati-Rad, M. Karimi, M. Rezaeivala, Synthesis and Characterization of a Novel Ligand and Spectroscopic Study of the Formation of its Complexes with Different Cations and Their Sensory Characteristics, J. Appl. Spectrosc. 84 (2018) 1089–1097, https://doi.org/10.1007/s10812-018-0593-9.
[14] M. Rezaeivala, H. Keypour, S. Salehzadeh, R. Latifi, F. Chalabian, F. Katouzian, Synthesis, characterization and crystal structure of some new Mn(II) and Zn(II) macroacyclic Schiff base complexes derived from two new asymmetrical (N5) branched amines and pyridine-2-carbaldehyde or O-vaniline and their antibacterial properties, J. Iran. Chem. Soc. 11 (2014) 431–440, https://doi.org/10.1007/s13738-013-0315-4.
[15] M. Rezaeivala, M. Ahmadi, B. Captain, M. Bayat, M. Saeidirad, S. Şahin-Bölükbaşı, B. Yıldız, R.W. Gable, Some new morpholine-based Schiff-base complexes; Synthesis, characterization, anticancer activities and theoretical studies, Inorganica Chim. Acta. 513 (2020), 119935, https://doi.org/10.1016/j.ica.2020.119935.
[16] M. Rezaeivala, M. Ahmadi, B. Captain, S. Şahin-Bölükbaşı, A.A. Dehghani-Firouzabadi, R.William Gable, Synthesis, characterization, and cytotoxic activity studies of new N4O complexes derived from 2-({3-[2-*morpholinoethylamino*]-N3-([*pyridine*-2-*yl*]methyl) propylimino} methyl)phenol, Appl. Organomet. Chem. 34 (2020) e5325, https://doi.org/10.1002/aoc.5325.
[17] S. Savir, Z.J. Wei, J.W.K. Liew, I. Vythilingam, Y.A.L. Lim, H.M. Saad, K.S. Sim, K. W. Tan, Synthesis, cytotoxicity and antimalarial activities of thiosemicarbazones and their nickel (II) complexes, J. Mol. Struct. 1211 (2020), 128090, https://doi.org/10.1016/j.molstruc.2020.128090.

[18] P. Shetty, Schiff bases: an overview of their corrosion inhibition activity in acid media against mild steel, Chem. Eng. Commun. 207 (2020) 985–1029, https://doi.org/10.1080/00986445.2019.1630387.
[19] D. Douche, H. Elmsellem, E.H. Anouar, L. Guo, B. Hafez, B. Tüzün, A. El Louzi, K. Bougrin, K. Karrouchi, B. Himmi, Anti-corrosion performance of 8-hydroxy-quinoline derivatives for mild steel in acidic medium: gravimetric, electrochemical, DFT and molecular dynamics simulation investigations, J. Mol. Liq. 308 (2020), 113042, https://doi.org/10.1016/j.molliq.2020.113042.
[20] B. TÜZÜN, Examination of anti-oxidant properties and molecular docking parameters of some compounds in human body, Turkish Comput. Theor. Chem. 4 (2020) 76–87, https://doi.org/10.33435/tcandtc.781008.
[21] M.J. Frisch, G.W. Trucks, H.B. Schlegel, G.E. Scuseria, M.A. Robb, J.R. Cheeseman, G. Scalmani, V. Barone, B. Mennucci, G.A. Petersson, H. Nakatsuji, M. Caricato, X. Li, H.P. Hratchian, A.F. Izmaylov, J. Bloino, G. Zheng, J.L. Sonnenberg, M. Hada, M. Ehara, K. Toyota, R. Fukuda, J. Hasegawa, M. Ishida, T. Nakajima, Y. Honda, O. Kitao, H. Nakai, T. Vreven, J.A. Montgomery, J.E. Peralta, F. Ogliaro, M. Bearpark, J.J. Heyd, E. Brothers, K.N. Kudin, V.N. Staroverov, R. Kobayashi, J. Normand, K. Raghavachari, A. Rendell, J.C. Burant, S.S. Iyengar, J. Tomasi, M. Cossi, N. Rega, J.M. Millam, M. Klene, J.E. Knox, J.B. Cross, V. Bakken, C. Adamo, J. Jaramillo, R. Gomperts, R.E. Stratmann, O. Yazyev, A.J. Austin, R. Cammi, C. Pomelli, J.W. Ochterski, R.L. Martin, K. Morokuma, V.G. Zakrzewski, G.A. Voth, P. Salvador, J.J. Dannenberg, S. Dapprich, A.D. Daniels, O. Farkas, J. B. Foresman, J.V. Ortiz, J. Cioslowski, D.J. Fox, Gaussian 09, Revision D.01, Gaussian Inc, Wallingford CT, 2009.
[22] S. Satpati, S.K. Saha, A. Suhasaria, P. Banerjee, D. Sukul, Adsorption and anti-corrosion characteristics of vanillin Schiff bases on mild steel in 1M HCl: experimental and theoretical study, RSC Adv 10 (2020) 9258–9273, https://doi.org/10.1039/c9ra07982c.
[23] M.J. Frisch, G.W. Trucks, H.B. Schlegel, G.E. Scuseria, M.A. Robb, J.R. Cheeseman, G. Scalmani, V. Barone, B. Mennucci, G.A. Petersson, Gaussian 09. 2009, Gaussian, Inc. Wallingford, Ct, USA, 1990, p. 542.
[24] K. Alaoui, A. Abousalem, B. Tüzün, Y. El Kacimi, Triazepines compounds as novel synthesized corrosion inhibitors, IGI Glob (2020) 156–186, https://doi.org/10.4018/978-1-7998-2775-7.ch007.
[25] K. Vimal, R.B.V. Appa, Chemically modified biopolymer as an eco-friendly corrosion inhibitor for mild steel in a neutral chloride environment, New J. Chem. 41 (2017) 6278–6289, https://doi.org/10.1039/c7nj00553a.
[26] W. Al Zoubi, S.G. Mohamed, A.A.S. Al-Hamdani, A.P. Mahendradhany, Y.G. Ko, Acyclic and cyclic imines and their metal complexes: recent progress in biomaterials and corrosion applications, RSC Adv 8 (2018) 23294–23318, https://doi.org/10.1039/C8RA01890A.
[27] I. Correia, J. Costa Pessoa, M.T. Duarte, M.F.M. Da Piedade, T. Jackush, T. Kiss, M. M.C.A. Castro, C.F.G.C. Geraldes, F. Avecilla, Vanadium(IV and V) complexes of Schiff bases and reduced Schiff bases derived from the reaction of aromatic o-hydroxyaldehydes and diamines: synthesis, characterisation and solution studies, Eur. J. Inorg. Chem. (2005) 732–744, https://doi.org/10.1002/ejic.200400481.
[28] A. Heidarpour, Z.S. Mousavi, S. Karimi, S.M. Hosseini, On the corrosion behavior and microstructural characterization of Al2024 and Al2024/Ti_2SC MAX phase surface composite through friction stir processings, J. Appl. Electrochem. (2021) 1–14, https://doi.org/10.1007/s10800-021-01567-9.
[29] E. Alibakhshi, M. Ramezanzadeh, G. Bahlakeh, B. Ramezanzadeh, M. Mahdavian, M. Motamedi, Glycyrrhiza glabra leaves extract as a green corrosion inhibitor for mild steel in 1M hydrochloric acid solution: experimental, molecular dynamics, Monte Carlo and quantum mechanics study, J. Mol. Liq. 255 (2018) 185–198, https://doi.org/10.1016/j.molliq.2018.01.144.
[30] M. Bobina, A. Kellenberger, J.P. Millet, C. Muntean, N. Vaszilcsin, Corrosion resistance of carbon steel in weak acid solutions in the presence of L-histidine as corrosion inhibitor, Corros. Sci. 69 (2013) 389–395, https://doi.org/10.1016/j.corsci.2012.12.020.